Circuits Syst Signal Process (2012) 31:1279–1296
DOI 10.1007/s00034-012-9392-3

Circuits with Oscillatory Hierarchical Farey Sequences and Fractal Properties

Wieslaw Marszalek

Received: 25 March 2011 / Revised: 17 January 2012 / Published online: 10 February 2012

Abstract We present two dual oscillating circuits having a wide spectrum of dynamical properties but relatively simple topologies. Each circuit has five bifurcating parameters, one nonlinear element of cubic current–voltage characteristics, one controlled element, LCR components and a constant biasing source. The circuits can be considered as two coupled oscillators (linear and nonlinear) that form dual *jerk* circuits. Bifurcation diagrams of the circuits show a rather surprising result that the bifurcation patterns are of the Farey sequence structure and the circuits' dynamics is of a fractal type. The circuits' fractal dimensions of the box counting (capacity) algorithm, Kaplan–Yorke (Lyapunov) type and its modified (improved) version are all estimated to be between 2.26 and 2.52. Our analysis is based on numerical calculations which confirm a close relationship of the circuits' bifurcation patterns with those of the Ford circles and Stern–Brocot trees.

Keywords Oscillating circuits · Bifurcations · Singularly perturbed systems · Farey sequence · Stern–Brocot tree · Ford circles · Fractals

1 Introduction

In the earlier paper [16] two dual circuits similar to those shown in Fig. 1 (without the coupling conductance G and resistance R) were investigated from the point of view of their mixed-mode oscillations (MMOs), canard solutions and folded points of the corresponding system of differential-algebraic equations (DAEs).

Mathematical model of such circuits comprises two linear and one nonlinear ordinary differential equations (ODEs). Such a model was also investigated in [9] and

W. Marszalek (✉)
College of Engineering and Information Sciences, DeVry University, 630 US Highway 1, North Brunswick, NJ 08902, USA
e-mail: wmarszalek@devry.edu

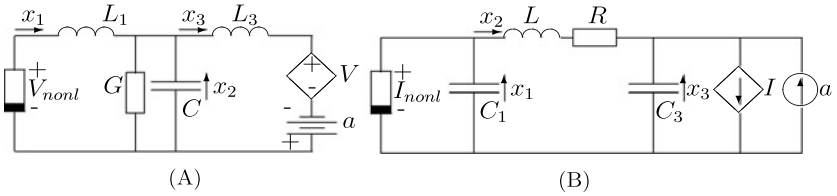

Fig. 1 (**A**) The LCL circuit with $L_1 = \epsilon \ll 1$, $V = (1+b)x_2$, $V_{\text{nonl}} = \alpha x_1^2 + \beta x_1^3$. (**B**) The CLC circuit with $C_1 = \epsilon \ll 1$, $I = (1+b)x_2$, $I_{\text{nonl}} = \alpha x_1^2 + \beta x_1^3$. For both circuits: $a > 0$, $b > 0$, $\beta < 0$ and $\alpha > 0$

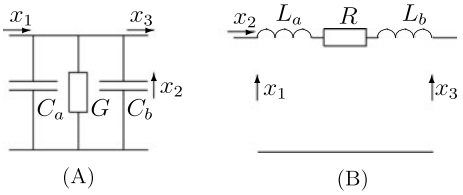

Fig. 2 Coupling of oscillators through conductance G and resistance R. The coupling is of full strength if $G = 0$ for circuit **A** (equivalently $R = 0$ for circuit **B**) while the oscillators are completely decoupled if $G \to \infty$ (equivalently $R \to \infty$)

several conclusions about the occurrence of the L^s patterns (large and small amplitude oscillations, or LAOs and SAOs, respectively) were drawn.

Each of the two circuits in Fig. 1 can be considered as a coupling of two oscillators (nonlinear and linear ones). The nonlinear oscillator comprises a nonlinear element with a cubic characteristics V_{nonl} (or I_{nonl}), an inductor (Fig. 1(A)) or a capacitor (Fig. 1(B)), while the linear oscillator includes an inductor, a capacitor, a voltage controlled voltage source (or a current controlled current source) and a biasing constant voltage (or current) source. The inductance L and capacitance C in the circuits in Fig. 1 are split between the two oscillators as shown in Fig. 2 with $C_a + C_b = C$ and $L_a + L_b = L$.

If we assume that $0 < L_1 \equiv \epsilon \ll 1$ and $C, L_2 \sim \mathcal{O}(1)$ for the circuit in Fig. 1A ($0 < C_1 \equiv \epsilon \ll 1$ and $L, C_2 \sim \mathcal{O}(1)$ for the circuit in Fig. 1B), then both circuits can be described by the singularly perturbed model

$$\begin{aligned} \epsilon x_1' &= -x_2 + \alpha x_1^2 + \beta x_1^3 \equiv g(x_1, x_2, x_3) \\ x_2' &= x_1 - x_3 - K x_2 \equiv f_1(x_1, x_2, x_3) \\ x_3' &= a - b x_2 \equiv f_2(x_1, x_2, x_3) \end{aligned} \tag{1}$$

where $K \equiv G$ for the circuit in Fig. 1A and $K \equiv R$ for the circuit in Fig. 1B.

As reported in [9, 16], the MMOs phenomenon (a combination of LAOs and SAOs) may include oscillations with quite complex patterns. The SAOs trace the weak canard trajectory of (1) around the origin $(0, 0, 0)$, while the LAOs are due to the cubic nonlinearity and *return mechanism*. Canard trajectories (weak and strong) are closely related to certain folded nodes of DAEs that one obtains from (1) by assuming $\epsilon = 0$. Furthermore, a desingularization process of DAEs results in a system of two ODEs with a folded nodal point. See [1, 2, 6, 10, 13–15, 19, 21, 23] for more details of these properties.

It is known that (1) is a prototypical model of mixed-mode oscillations with three time scales. Since a and b in (1) are usually of order ϵ, therefore one can consider

x_1, x_2 and x_3 as the *fastest*, *medium* and *slowest* variables, respectively. Two time scales are also possible to achieve in (1) by an appropriate choice of parameters. Many practical oscillating systems in chemistry, physics and neuroscience have multiple time scales, exhibit MMOs and chaos (e.g. the Belousov–Zhabotinski reaction, Bonhoeffer–van der Pol oscillator, neuron oscillations in human brain and others [6]).

In this paper we further analyze the two circuits in Fig. 1. The MMOs are not the only possible dynamical features of the circuits. In fact, all the parameters α, β, a, b and K in (1) may be considered as the bifurcation parameters. We shall analyze the local maximum values of LAOs and SAOs and show that, by slowly changing any of the above parameters, we can obtain the local maximum values of $x_i(t)$, $i = 1, 2, 3$, that can be described by the Farey arithmetic [17] and related to the Stern–Brocot tree [8, 24]. In our analysis we use the letters L and s in L^s to describe the *number of local maximum values* of the steady-state LAOs and SAOs, respectively, and not the number of LAOs and SAOs. Thus, our L^s is different from the L^s used, for example, in [9, 16]. Through a series of numerical experiments we shall show that the L^s oscillations for the circuits in Fig. 1 occur in the order of Farey sequence of coprime integers. Also, the circuits can be considered as ones having a chaotic strange attractor, and as such can be characterized by a special number called the fractal dimension. Various fractal dimensions of the circuits in Fig. 1 are discussed in Sects. 3 and 4.

The paper is written for the purpose of showing how relatively simple circuits with one nonlinear element exhibit an amazing spectrum of dynamical properties ranging from MMOs, through chaotic responses, various bifurcation diagrams related to the Farey sequence of coprime integers, to fractal properties. We also propose a new bifurcation tree illustrating a hierarchical structure in which the circuits oscillate (see Figs. 12 and 13 to follow). We also show a relationship between the dynamical properties of (1) and Newton's second law (in Sect. 4.3), allowing for a "mechanical" interpretation of x_1, x_1' and x_1'' as "position", "velocity" and "acceleration," respectively. It is our belief that the circuits analyzed in this paper could become benchmark examples of nonlinear circuits' studies.

The circuits shown in Fig. 1 also fall into the category of chaotic *jerk* circuits [22], that is, the circuits described by a nonlinear third order equation in the form $x''' = J(x'', x', x)$. The nonlinear function J is called a *jerk* since, in mechanical systems, it would correspond to the first derivative of acceleration of $x(t)$. The *jerk* structure of (1) follows from the fact that variable $x_1(t)$ in (1) satisfies the following equation:

$$x_1'' + \left(K - \epsilon^{-1}\left(2\alpha x_1 + 3\beta x_1^2\right)\right)x_1' + \epsilon^{-1}\left(x_1 - K\left(\alpha x_1^2 + \beta x_1^3\right)\right) = \epsilon^{-1}x_3(t) \quad (2)$$

which is coupled with the first-order equation

$$x_3' - b\epsilon x_1' = a - b\left(\alpha x_1^2 + \beta x_1^3\right). \quad (3)$$

From (2) and (3) we obtain the *jerk* equation in variable x_1

$$x_1''' + \left[K - \epsilon^{-1}N'(x_1)\right]x_1'' + \left[-\epsilon^{-1}N''(x_1)x_1' + \epsilon^{-1} - \epsilon^{-1}KN'(x_1) - b\right]x_1' - \epsilon^{-1}a + \epsilon^{-1}bN(x_1) = 0 \quad (4)$$

where $N(x_1) \equiv \alpha x_1^2 + \beta x_1^3$.

Alternatively, one can consider the second-order equation $x_3'' + Kx_3' - bx_3 = Ka - x_1$ coupled with (3). This gives another *jerk* equation in variable x_3, as follows:

$$x_3''' + Kx_3'' + \left(\epsilon^{-1} - b\right)x_3' - \epsilon^{-1}a + \epsilon^{-1}bN\left(\left(-x_3'' - Kx_3' + bx_3 + Ka\right)/b\right) = 0 \tag{5}$$

This equation is structurally different from the *jerk* equation (4). We comment about this difference and further properties of both *jerk* equations in Sect. 4.

The paper is organized as follows. In Sect. 2 we present numerically obtained representative bifurcation diagrams when parameters α, β, a and b vary. In Sect. 3 we compare the hierarchical oscillations of the circuits to the Farey sequences, Stern–Brocot trees and Ford circles. After analyzing several bifurcation diagrams, we also estimate the circuits' counting box fractal dimension in Sect. 3. Then, we construct our own tree with hierarchical windows of a fractal nature. In the infinite sequence of such windows we focus on those windows denoted by 2^k, k being a positive odd integer, as they are formed in the shape of the Stern–Brocot trees. We discuss and compare the circuits' fractal counting box, Kaplan–Yorke and modified (improved) Kaplan–Yorke dimensions in Sect. 4. The *jerky* Newtonian nature of (4) and its relationship to Newton's second law $F = mx''$ is also discussed in Sect. 4. Finally, we draw our conclusions in Sect. 5. Throughout the paper the symbol $\oplus$ stands for the following operation on four integers p_1, q_1, p_2 and q_2: $p_1/q_1 \oplus p_2/q_2 = (p_1 + p_2)/(q_1 + q_2)$.

2 Bifurcation Diagrams

The three basic modes of operation of the circuits are illustrated in Fig. 3 [16] which shows the time series and 2D solutions of (1) with $\epsilon = 0.01$, $\alpha = 1.5$, $\beta = -1$, $b =$

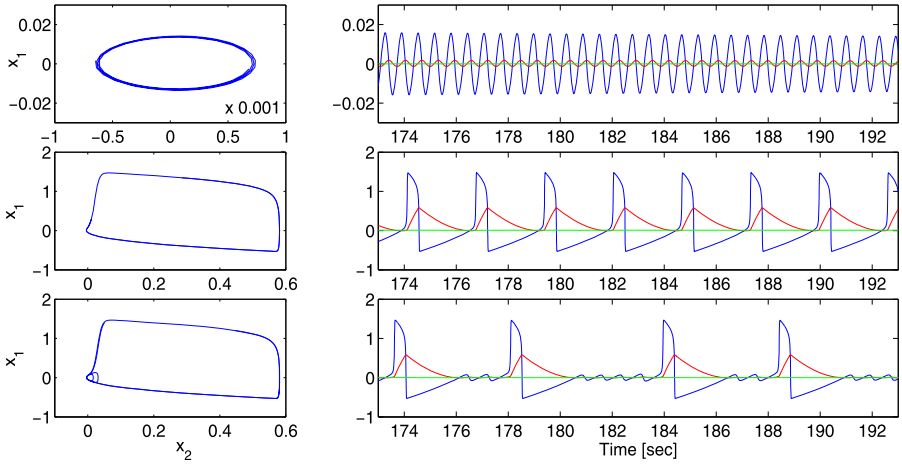

Fig. 3 (Color online) *Left column*: x_1 versus x_2; *right column*: time responses ($172 \le t \le 194$); both columns: SAOs only (*top*: $a = 0$), LAOs only (*middle*: $a = 0.00105$) & MMOs (*bottom*: $a = 0.00055$) with x_1 (*blue*), x_2 (*red*), x_3 (*green*)

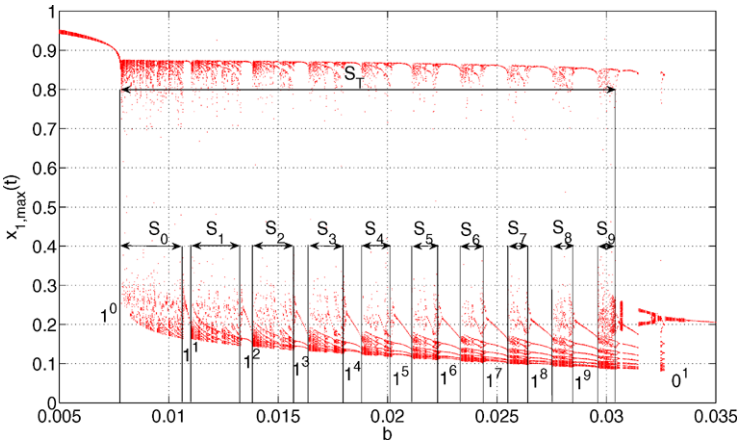

Fig. 4 Bifurcation diagram for $\alpha = 1$, $\beta = -1$, $a = 0.0005$, $\epsilon = 0.01$, $K = 0.3$ and $0.005 < b < 0.035$ with intervals of MMOs sequence $1^0 \to 1^1 \to 1^2 \to \cdots \to 1^9 \to 0^1$

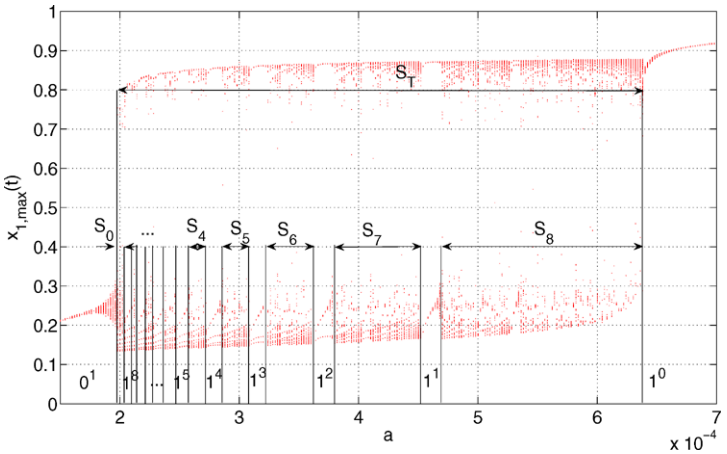

Fig. 5 Bifurcation diagram for $\alpha = 1$, $\beta = -1$, $b = 0.005$, $\epsilon = 0.01$, $K = 0.3$ and $0.00015 < a < 0.0007$ with intervals of MMOs sequence $0^1 \to 1^8 \to 1^7 \to \cdots \to 1^1 \to 1^0$

0.005, $K = 0$ and three values of a. In the SAOs only case, the small amplitude oscillations around the origin $(0, 0, 0)$ are due to the Hopf bifurcation for $a = 0$. We used non-zero initial conditions only for the SAOs case in the top panel in Fig. 3. In all other calculations in this paper the initial conditions were all zero.

In the LAOs only case, a trajectory bypasses the region of small amplitude oscillations around the origin. The MMOs case is in some sense a combination of the previous two cases. The mechanism in which SAOs and LAOs occur is quite complex and has been the topics of recent papers [2, 6, 9, 10, 16, 19, 23].

The occurrence of MMOs is not the only interesting feature of the circuits in Fig. 1. When parameters α, β, a or b change slowly, system (1) may bifurcate and show complex chaotic behavior with MMOs transitions of various types. Figures 4, 5, 6, 7

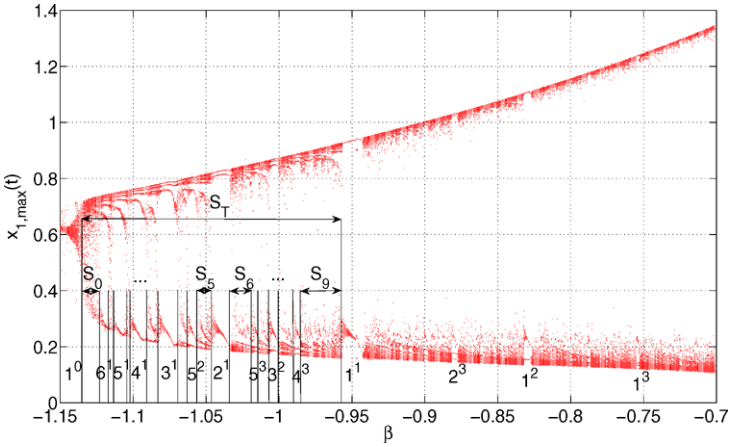

Fig. 6 Bifurcation diagram for $\alpha = 1$, $a = 0.0005$, $b = 0.005$, $\epsilon = 0.01$, $K = 0.3$ and $-1.15 < \beta < -0.70$ with intervals of MMOs sequence $1^0 \to 6^1 \to 5^1 \to \cdots \to 1^1 \to 1^2 \to 1^3$

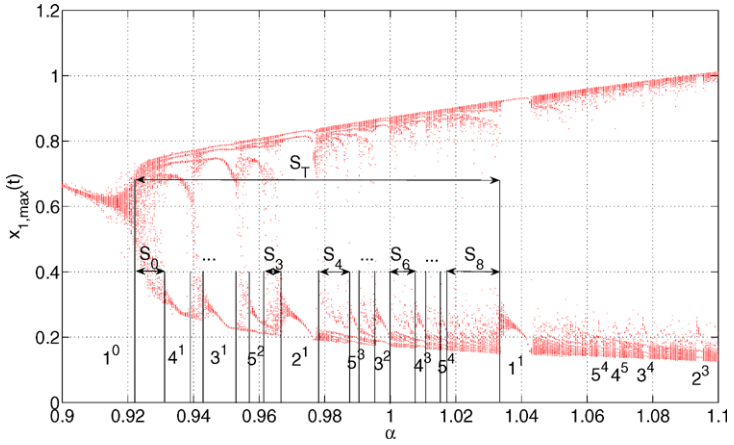

Fig. 7 Bifurcation diagram for $\beta = -1$, $a = 0.0005$, $b = 0.005$, $\epsilon = 0.01$, $K = 0.3$ and $0.9 < \alpha < 1.1$ with intervals of MMOs sequence $1^0 \to 4^1 \to \cdots \to 1^1 \to \cdots \to 2^3$

show typical bifurcation diagrams with the vertical axis representing the maximum values of $x_1(t)$ identified in the interval $300 \leq t \leq 500$. All calculations were done for $0 \leq t \leq 500$ (with zero initial conditions), but the interval $0 \leq t < 300$ was not used in the process of identifying the maximum values of $x_1(t)$. Throughout the whole analysis we kept the value of ϵ unchanged at 0.01.

Bifurcation diagram in Fig. 4 clearly shows a pattern of sequence $1^0 \to 0^1$ (through a series of oscillations: $1^0 \to 1^1 \to 1^3 \to \cdots \to 0^1$), while the sequence in Fig. 5 is of type $0^1 \to 1^0$. On the other hand, Figs. 6 and 7 show the sequence of local maximum values $1^0 \to 1^1$ with a few additional values of L^s to the right of 1^1. The intervals S_i will be used in the sequel to determine the fractal dimensions of the circuits, as a detailed analysis of the L^s patterns clearly indicates that the patterns

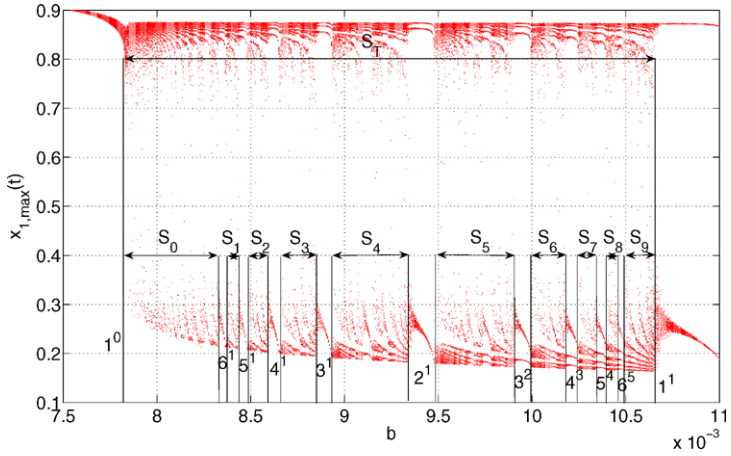

Fig. 8 Detailed bifurcation sequence of MMOs $1^0 \rightarrow 1^1$ with several lower level hierarchical oscillations (interval S_0 in Fig. 4)

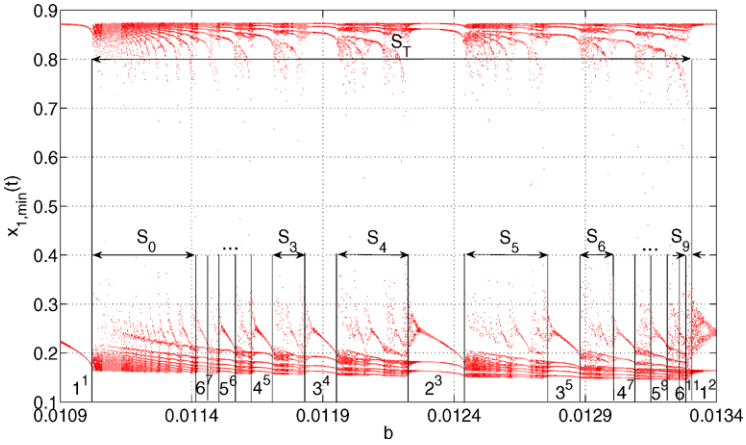

Fig. 9 Detailed bifurcation sequence of MMOs $1^1 \rightarrow 1^2$ with several lower level hierarchical oscillations (interval S_1 in Fig. 4)

are directly linked to the Farey sequence of the pairs of coprime integers (see the L^s values shown in Figs. 4, 5, 6, 7 and in Figs. 8, 9, 10, 11, which follow). As a consequence, we shall conjecture that the dynamics of the circuits in Fig. 1 is in fact of a fractal type. Next, we shall use the bifurcation diagrams with varying b to proceed with a more detailed analysis.

3 Fractal Windows and Trees

First, when a resolution of computation is increased, one can obtain more detailed bifurcation diagrams for any of the ten intervals S_i in Fig. 4. Figures 8, 9, 10, 11

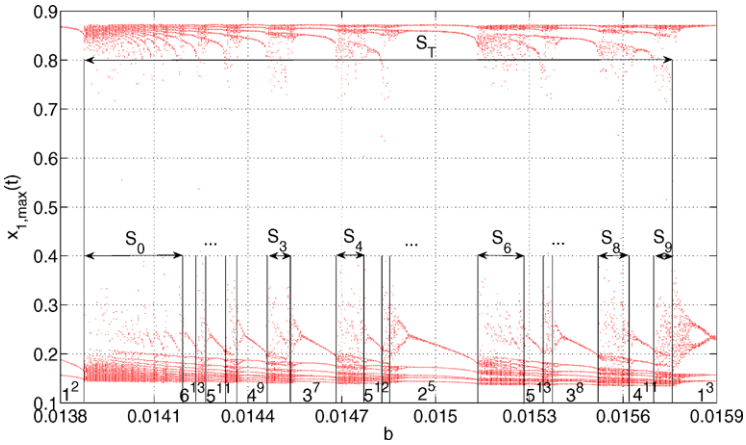

Fig. 10 Detailed bifurcation sequence of MMOs $1^2 \rightarrow 1^3$ with several lower level hierarchical oscillations (interval S_2 in Fig. 4)

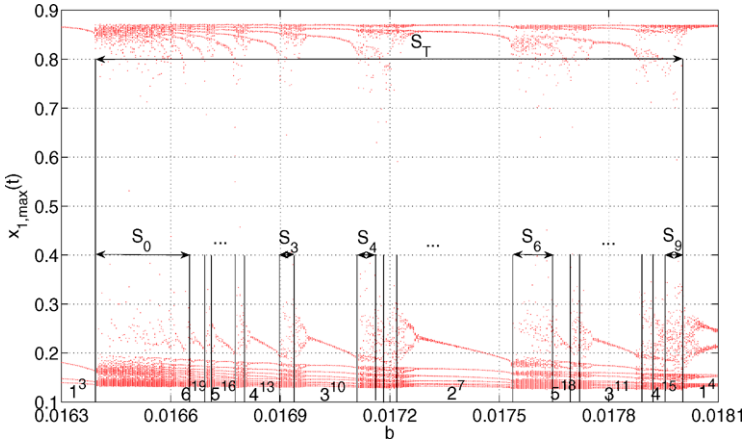

Fig. 11 Detailed bifurcation sequence of MMOs $1^3 \rightarrow 1^4$ with several lower level hierarchical oscillations (interval S_3 in Fig. 4)

show four such diagrams. These graphs yield a graphical representation of the first several layers of the L^s sequences as is shown in Fig. 12. This tree is a modification of the Farey and Stern–Brocot trees [8, 24] and also corresponds to the Ford circles [7]. Any pair of coprime integers L^s is marked in Fig. 12 as a single $\times$ point with its horizontal coordinate $L/(L+s)$, sometimes called the firing number. The vertical coordinate depends on the window to which the pair L^s belongs. For fixed values of coprime integers L and s, the tree in Fig. 12, just like the Farey sequence, includes all possible coprimes between L^s and s^L. The pairs of coprimes between L^s and s^L (coprimes at the same vertical level in Fig. 12) belong to different consecutive windows. For instance, at the vertical level 8 we have all coprimes between 1^8 and 8^1 in the following sequence: 1^8, 2^{13}, 3^{17}, 3^{16}, 4^{19}, 4^{17}, 5^{19}, 5^{18}, 5^{17}, 5^{16}, 6^{17}, …, 8^7,

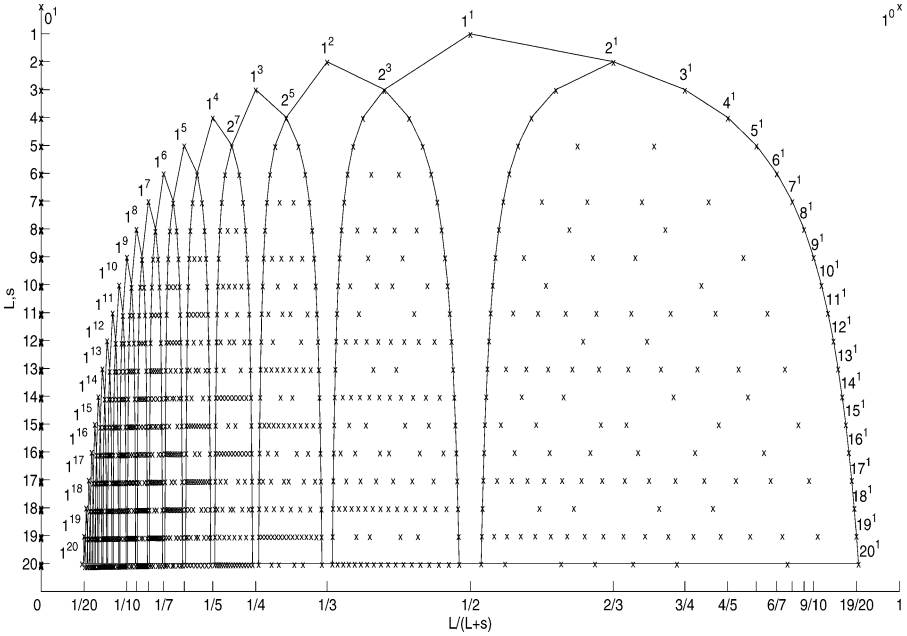

Fig. 12 Bifurcation tree with L^s, $L \le 20$, $s \le 20$: each window 1^k, $k = 1, 2, \ldots, 20$, comprises two disjoint windows 2^n and 2^l such that $\frac{1}{k} = \frac{2}{n} \oplus \frac{2}{l}$ (e.g. the 1^1 window comprises windows 2^1 and 2^3 with $\frac{1}{1} = \frac{2}{1} \oplus \frac{2}{3} = \frac{4}{4}$). Also, each 2^k window comprises two disjoint windows 3^n and 3^l such that $\frac{2}{k} = \frac{3}{n} \oplus \frac{3}{l}$, etc. Within each window the L^s elements at the same horizontal level have the same L value, their respective s values run through all possible integer values such that g.c.d.$(L, s) = 1$ and $\sum_m \oplus L_m/s_m = L/s$ (e.g. the 2^3 window includes the elements 8^{15}, 8^{13}, 8^{11} and 8^9 at the level marked *9* with $\frac{8}{15} \oplus \frac{8}{13} \oplus \frac{8}{11} \oplus \frac{8}{9} = \frac{32}{48} = \frac{2}{3}$). Other similarity patterns also exist for this tree, including vertical patterns within each window. See Fig. 13 with a partial illustration of such a vertical pattern for the 2^1 window. Also, each window 2^k has a pattern of elements as shown in Fig. 15. This tree is, if fact, the Stern–Brocot tree [24]

8^5, 8^3, 8^1, with their increasing firing numbers 1/9, 2/15, 3/20, 3/19, 4/23, 4/21, 5/24, 5/23, 5/22, 5/21, 6/23, …, 8/15, 8/13, 8/11, 8/9. Also, the coprimes 8^1, 8^3, 8^5, 8^7 are located inside the window 2^1 (because $(8+8+8+8)/(1+3+5+7) = 2/1$, see the vertical level 8). The coprimes 8^9, 8^{11}, 8^{13}, 8^{15} are located inside the window 2^3 (because $(8+8+8+8)/(9+11+13+15) = 2/3$, see the vertical level 9), etc. The total number of coprime pairs 8^s within each window equals $\varphi(8) = \varphi(2^3) = 4$, where $\varphi(n)$ is Euler's totient function [7]. Similarly, the total number of coprime pairs 15^s within each window is $\varphi(15) = \varphi(3)\varphi(5) = 8$. For example, in the window 2^1 we have the coprimes 15^1, 15^2, 15^4, 15^7, 15^8, 15^{11}, 15^{13}, 15^{14} which yield $15^1 \oplus 15^2 \oplus 15^4 \oplus 15^7 \oplus 15^8 \oplus 15^{11} \oplus 15^{13} \oplus 15^{14} = \frac{8\times15}{16+17+19+22+23+26+28+29} = \frac{2}{3}$, which is the firing number for 2^1. This sequence of coprime pairs 15^s continues in window 2^3 with the coprimes 15^{16}, 15^{17}, 15^{19}, 15^{22}, 15^{23}, 15^{26}, 15^{28}, 15^{29} which result (with the $\oplus$ operation) in value 2/5, that is, the firing number of 2^3. This pattern continues indefinitely for windows 2^5, 2^7, …. The hierarchical oscillating sequences of L^s grouped by windows in Fig. 12 (also in Fig. 13) are interesting as each of the

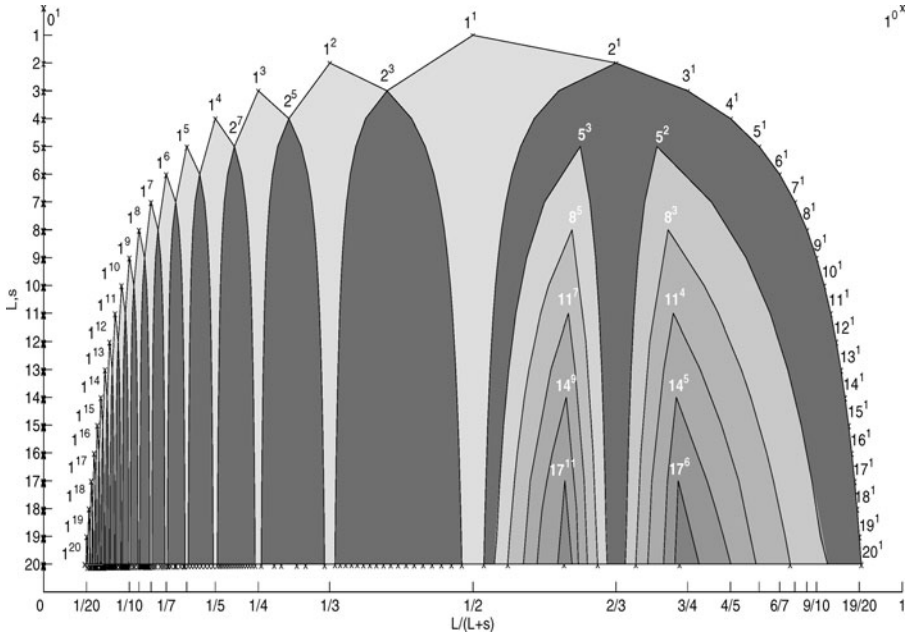

Fig. 13 Bifurcation tree as in Fig. 12 with a pattern of vertically overlapping windows inside 2^1. The same pattern exists for all windows 2^k, $k \geq 1$ and odd. There are no numbers L^s in the areas of *light-shaded tongues* of 1^k. Each *dark-shaded* window can also be subsequently partition into *light-shaded* tongues and *dark-shaded* windows

2^k (k being odd positive) windows is in fact the Stern–Brocot tree [24]. We discuss this relationship later on.

We begin with the bifurcation diagram in Fig. 4. Using the values of S_i and S_T one can solve the following equation to compute the fractal dimension, D [17]:

$$\sum_{i=0}^{n} (S_i/S_T)^D = 1. \tag{6}$$

Equation (6) is known as the box counting (capacity) formula with D called the counting box (capacity) fractal dimension [4]. In our computations we have chosen $i = 0, \ldots, 9$, that is, 10 intervals S_i between various L^s sequences, as shown in Figs. 4, 8–11. Equation (6) for the diagram in Fig. 4 is

$$0.1217^D + 0.0986^D + 0.0842^D + 0.0717^D + 0.0609^D + 0.0538^D + 0.0484^D + 0.0448^D + 0.0412^D + 0.0376^D = 1$$

which yields $D = 0.8449$. Due to a certain degree of uncertainty associated with a precise estimation of the boundaries of S_i and S_T in our bifurcation diagrams, it is impossible to compute the exact value of D, but we conjecture (based on further analysis) that the counting box (capacity) dimension for each of the three variables $x_i(t)$, $i = 1, 2, 3$ is about 0.84. This statement follows from the examination of the diagrams in Figs. 4, 8–11 and also those in Figs. 16 and 17 to be done later. Table 1

Table 1 Fractal dimensions D (6)

Figure	$L_1^{s_1} \to L_2^{s_2}$	D
Fig. 11	$1^3 \to 1^4$	0.7031
Fig. 10	$1^2 \to 1^3$	0.7307
Fig. 9	$1^1 \to 1^2$	0.8010
Fig. 8	$1^0 \to 1^1$	0.8179
Fig. 4	$1^0 \to 0^1$	0.8449

Table 2 Comparison of D: circuits and Ford circles

Figure	$L_1^{s_1} \to L_2^{s_2}$	D	Circles p^q	D
Fig. 4	$1^0 \to 0^1$	0.8449	$1^1, 1^2, 1^3, 1^4, 1^5, 1^6, 1^7, 1^8, 1^9$	0.8498
Fig. 5	$0^1 \to 1^0$	0.8443	$1^8, 1^7, 1^6, 1^5, 1^4, 1^3, 1^2, 1^1$	0.8496
Fig. 6	$1^0 \to 1^1$	0.7967	$1^1, 4^3, 3^2, 5^3, 2^1, 5^2, 3^1, 4^1, 5^1, 6^1$	0.8024
Fig. 7	$1^0 \to 1^1$	0.7919	$1^1, 5^4, 4^3, 3^2, 5^3, 2^1, 5^2, 3^1, 4^1$	0.8016

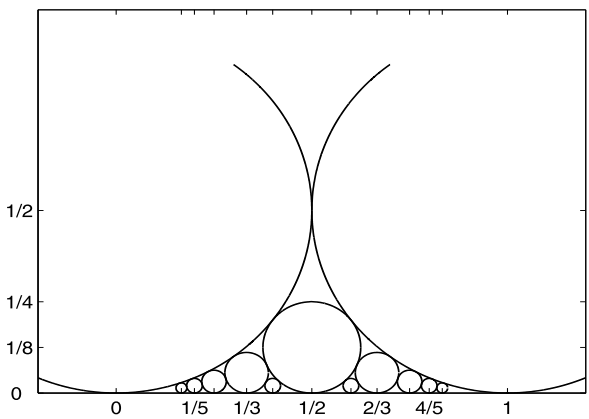

Fig. 14 Several Ford circles with $0 \le p/q \le 1$. More Ford circles with $p/q > 1$ can be found in [24]

shows several estimates of the values of D based on (6) and the five bifurcation diagrams with varying parameter b. Further comparison of the fractal dimension D for the circuits and the fractal dimension of the sequences of Ford circles p/q (see Fig. 14) is given in Table 2. We only use the Ford circles with $0 \le p/q \le 1$ since all the sequences L^s (marked as points $\times$ in Fig. 12) have their first coordinate between 0 and 1. For example, the three L^s sequences 2^3, 2^1 and 3^1 have their representative points $\times$ with the first coordinates $2/5$, $2/3$ and $3/4$, respectively (see Fig. 12).

The fractal dimension values in Table 2 of such different fractal objects (circuits and Ford circles) are surprisingly in a very good agreement. It is also known that the total area of all Ford circles for $0 < p/q < 1$ (therefore the fractal dimension of the Ford circles) can be computed as follows. Since the Ford circles associated with

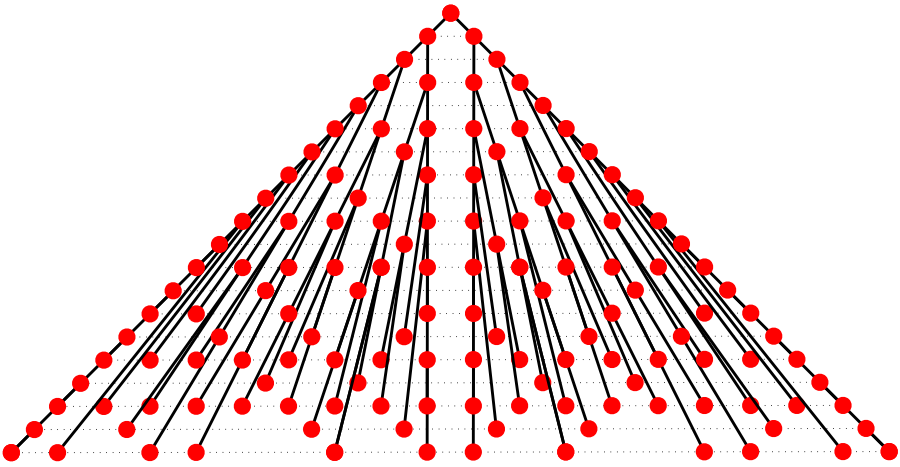

Fig. 15 (Color online) General structure of all windows 2^k in Fig. 12 (Stern–Brocot tree [24]). The *top red dot* corresponds to the top 2^k point of each window followed by horizontal segments with $2, 2, 4, 2, 6, 4, 6, 4, 10, \ldots$ points. This sequence of numbers is equivalent to the values of Euler's totient function $\varphi(n)$, $n = 2, 3, \ldots$

fractions $0 < p/q < 1$, g.c.d.$(p, q) = 1$, are centered at $(p/q, 1/(2q^2))$ and have their radii equal $1/(2q^2)$ (see Fig. 14), therefore the total area of such circles is[1]

$$A = \sum_{q\geq 1} \sum_{\substack{1\leq p<q \\ g.c.d.(p,q)=1}} \frac{\pi}{(2q^2)^2} = \frac{\pi}{4} \sum_{q\geq 1} \frac{1}{q^4} \sum_{\substack{1\leq p<q \\ g.c.d.(p,q)=1}} 1 \tag{7}$$

Using the Euler's totient and Riemann zeta functions, φ and ζ, respectively, we obtain

$$A = \frac{\pi}{4} \sum_{q\geq 1} \frac{\varphi(q)}{q^4} = \frac{\pi\zeta(3)}{4\zeta(4)} = \frac{45\zeta(3)}{2\pi^3} \approx 0.8723 \tag{8}$$

where $\zeta(4) = \pi^4/90$ was used.

Next, it is interesting to notice that each of the windows 2^k in Fig. 12 is in fact the Stern–Brocot tree. If we consider each such window as a polygon with the top point 2^k and the distance between the boundary points on the left and right sides of the window to be 1, then each window 2^k can be represented by the tree shown in Fig. 15. This is the Stern–Brocot tree. All the coprime pairs (L, s) represented by the $\times$ sign in Fig. 12 are now the red dots (color online) in Fig. 15. The tree in Fig. 15 has hierarchical symmetries corresponding to the symmetries of the internal (smaller) windows of each 2^k window. For example, by selecting the window 2^1 in Fig. 12 we

[1]For the analysis in this paper it suffices to consider the Ford circles with $0 \leq p/q \leq 1$ only. Because of the structure of our windows in Figs. 12 and 13 with the horizontal axis between 0 and 1 (the first coordinate of each point $\times$ is $p/(p+q)$), for Ford circles p^q with $p < q$ we use radii $0.5q^{-2}$, while for those with $p > q$ the radii are $0.5(p+q)^{-2}$. This applies to some computations in Table 2. For example, the sequence of circles $1^1, 5^4, 4^3, 3^2, 5^3, 2^1, 5^2, 3^1, 4^1$ gives the total area: $(\pi/4)((1/1^2)^2 + (1/9^2)^2 + (1/7^2)^2 + (1/5^2)^2 + (1/8^2)^2 + (1/3^2)^2 + (1/7^2)^2 + (1/4^2)^2 + (1/5^2)^2) = 0.8016$.

see two subsequent internal windows 3^2 and 3^1. These two windows correspond to the left and right subtrees in Fig. 15. Each of the windows 3^2 and 3^1 has its own consecutive symmetry, etc. Infinite self-similarity fractal pattern is clearly seen in the splitting of the trees in Fig. 15.

4 More Estimates of Fractal Dimensions and Comparison with Other Chaotic Systems

4.1 Fractal Dimensions D_{KY} and D_{Σ}

By using the bifurcation diagram of $x_1(t)$ in Fig. 4 and formula (6) in Sect. 3 we estimated the counting box fractal dimension D to be 0.84. Bifurcation diagrams of the remaining variables $x_2(t)$ and $x_3(t)$ are shown in Figs. 16 and 17. If the formula (6) is applied to both of those diagrams, then one obtains the same values of the counting box fractal dimensions as we obtained for $x_1(t)$ ($D = 0.84$). Thus, all three variables together yield the counting box fractal dimension, say D_c, of the circuits as $D_c = 2.52$ (that is 3×0.84).

It is worth comparing the above fractal dimension with some of the other fractal dimensions used in the analysis of fractals. It is well know that the Kaplan–Yorke (Lyapunov) fractal dimension is a widely used one when the dynamical equations are available. For a three-variable nonlinear dynamical system with a strange attractor the Kaplan–Yorke dimension is found by numerically calculating the Lyapunov exponents λ_i, $i = 1, 2, 3$, and then using them in the formula [3]

$$D_{KY} = 1 - \frac{\lambda_1}{\lambda_3} \tag{9}$$

with $\lambda_1 > 0$, $\lambda_2 = 0$, $\lambda_3 < 0$ and $\lambda_1 + \lambda_3 < 0$ (conditions for the existence of strange attractor). On the other hand, the modified (improved) Kaplan–Yorke dimension, denoted by D_{Σ} results from a quadratic interpolation rather than a linear one used in

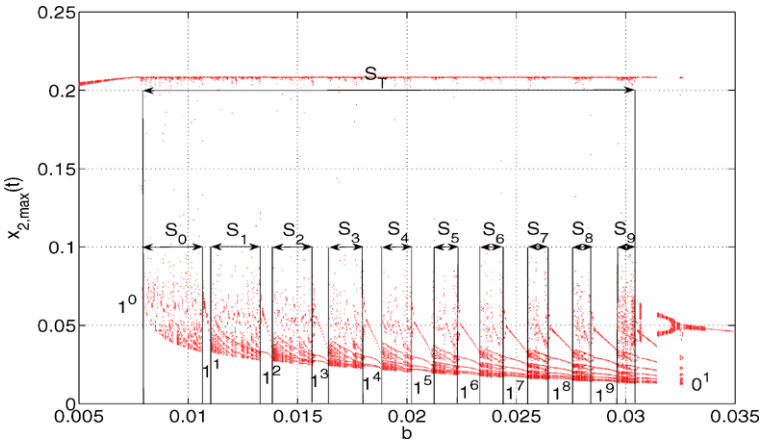

Fig. 16 Bifurcation sequence of MMOs $1^0 \to 1^1 \to \cdots \to 1^9 \to 0^1$ for $x_2(t)$ and the same parameters as in Fig. 4

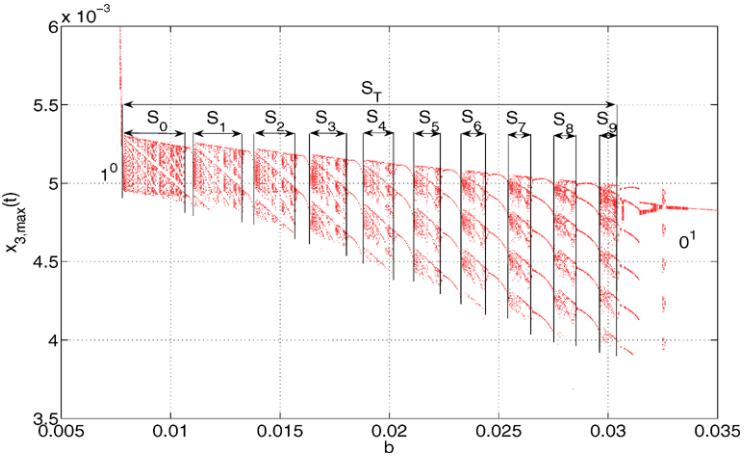

Fig. 17 Bifurcation sequence of MMOs $1^0 \to 1^1 \to \cdots \to 1^9 \to 0^1$ for $x_3(t)$ and the same parameters as in Fig. 4

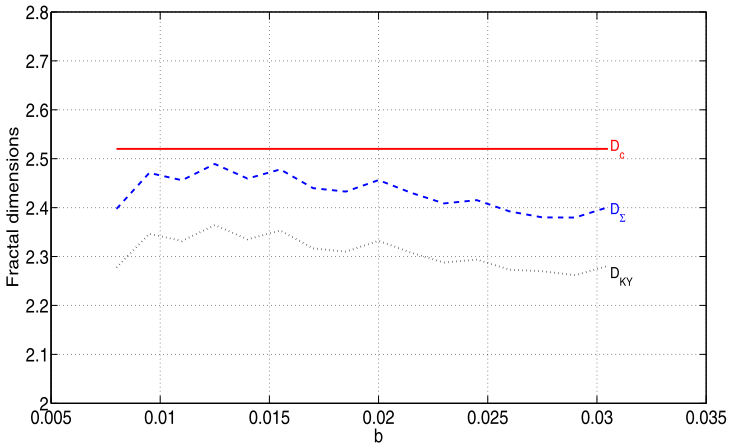

Fig. 18 Fractal dimensions $D_c = 2.52$ (const), D_Σ and D_{KY} with varying parameter b

deriving (9). In the three-variable chaotic flow with a strange attractor the D_Σ is computed from [3]

$$D_\Sigma = 1.5 + 0.5\sqrt{1 - 8\frac{\lambda_1}{\lambda_3}} \tag{10}$$

with $D_\Sigma \geq D_{KY}$ for $-1 \leq \lambda_1/\lambda_3 \leq 1$. The maximum difference $D_\Sigma - D_{KY}$ is $1/8$ and it occurs at $\lambda_1/\lambda_3 = -3/8$. Finally, it is known that for most chaotic flows we find that the Kaplan–Yorke and counting box (capacity) dimensions satisfy the following relation: $D_{KY} \leq D_\Sigma$.

To make our calculations comparable and consistent, we have used the same interval S_T (see Figs. 4, 16 and 17) to find D_{KY} and D_Σ for the circuits in Fig. 1. Figure 18

shows the D_c, D_{KY} and D_Σ (the two later dimensions vary with varying b). This figure certainly supports the generally accepted conjecture that $D_{KY} \le D_\Sigma \le D_c$.

4.2 Comparison of Fractal Dimensions

Fractal dimensions, in most cases, depend on the parameters and nonlinearities used. For example, in the case of Chua circuit, for most cases shown in Tables 1 and 2 in [20] we obtain the Kaplan–Yorke fractal dimensions, D_{KY}, in the interval 2.00–2.25, but there are also cases with D_{KY} equal 2.32, 2.40 or even 2.94. Other oscillators described by systems of three ODEs with only quadratic nonlinearities yield chaotic strange attractors with fractal dimensions D_{KY} that span practically the whole interval from 2 to 3. Those with values slightly greater than 2 come from simple flows with just one or two quadratic nonlinear terms in all three equations [18], while those systems with more quadratic terms yield higher values of D_{KY}, often between 2.5 and 3 [3]. The Rössler and Lorenz systems have their fractal dimensions of 2.01 and 2.06, respectively, since they contain only one (Rössler) and two (Lorenz) quadratic terms. On the other hand, the Newton–Leipnik system with three quadratic terms has D_{KY} between 2.24 and 2.30 (depending on parameters). The Rabinovich–Fabrikant system with five nonlinear terms has $D_{KY} = 2.30$ (for parameters $\gamma = 0.87, \alpha = 1.1$) [11]. The circuits studied in this paper have two nonlinear terms (quadratic, cubic) and their D_{KY} is between 2.26 and 2.36 (with varying parameter b, Fig. 18). This fits well with the general observation that simple three-variable ODEs with one or two nonlinear terms yield fractal dimensions D_{KY} closer to 2, while those with more nonlinear terms tend to have greater D_{KY}, around 2.5, 2.6, or closer to 3. Our system (1) falls in between: the system has slightly more complicated nonlinear terms than the Rössler and Lorenz systems, but still not too complicated to yield D_{KY} values above 2.5.

4.3 The *jerky* Newtonian Dynamics

The two *jerk* equations in the introductory section are quite different in nature with (4) being *jerky* Newtonian while (5) is not Newtonian. A *jerk* Newtonian equation originates from Newton's law $x'' - (1/m)F = 0$ to become $x''' - (1/m)(d/dt)F = 0$, where m is a mass and (d/dt) denotes the *total* derivative, yielding

$$x''' - \frac{1}{m}\big[(\partial_{x'}F)x'' + (\partial_x F)x' + \partial_t F\big] = 0. \tag{11}$$

Thus, from (4) we obtain

$$\begin{aligned} \partial_{x_1'}F &= m\big[\epsilon^{-1}N'(x_1) - K\big] \\ \partial_{x_1}F &= m\big[\epsilon^{-1}N''(x_1)x_1' - \epsilon^{-1} + \epsilon^{-1}KN'(x_1) + b\big] \\ \partial_t F &= m\big[\epsilon^{-1}a - \epsilon^{-1}bN(x_1)\big] \end{aligned} \tag{12}$$

and (12) yields the "acceleration" x_1'' $(= F/m)$ as follows:

$$\begin{aligned} F/m = \big[\epsilon^{-1}N'(x_1) - K\big]x_1' + \big(b - \epsilon^{-1}\big)x_1 + \epsilon^{-1}KN(x_1) \\ + \epsilon^{-1}at - \epsilon^{-1}b\int_0^t N\big(x_1(\tau)\big)d\tau + C \end{aligned} \tag{13}$$

where C is a constant.

It is easy to check from (12) that $\partial_{x_1 x_1'} F = \partial_{x_1' x_1} F = m\epsilon^{-1} N''(x_1)$. The integral term in (13) indicates that F depends not only on the instantaneous "position" $x_1(t)$ and "velocity" $x_1'(t)$, but also on the "memory" term $\epsilon^{-1} b \int_0^t N(x_1(\tau))d\tau$. This term depends on x_1, but not on x_1'. The *jerk* equation (4) is of polynomial and Newtonian type.[2]

Because of the nonlinear function $N(x_1) = \alpha x_1^2 + \beta x_1^3$, the *jerk* equation (5) is not linear in x_3''. Thus, (5) is of a polynomial, but not Newtonian type. One cannot find the F/m expression in the way it was possible for variable x_1. Also, it is not possible to find a single *jerk* equation for the remaining variable x_2. This is, again, due to the polynomial nonlinearity $\alpha x_1^2 + \beta x_1^3$ in (1). It remains to be seen what consequences of such a "mechanical" characterization of (1) are to the "electrical" variables x_1, x_2 and x_3 (currents and voltages). An application of the electromechanical Appell function seems to be of interest here and should shed more light on the *jerky* dynamics of (1) [25].

To compare, the celebrated Rössler system $x' = -y - ez$, $y' = x + ey$ and $z' = 1 + (x - c)z$ is *jerky* polynomial and Newtonian in y, *jerky* rational but not Newtonian in both x and z. The Lorenz systems is non-Newtonian in all three variables [12].

5 Conclusions

We have analyzed two dual circuits with one nonlinear element described by a cubic nonlinearity (parameters α and β), a linearly controlled voltage (current) source defined by parameter b, a small constant voltage (current) source (parameter a) and a linear coupling resistance (conductance) K. Each of those parameters can be considered as a bifurcation parameter. For particular sets of the five parameters we obtain various sequences of local maximum values corresponding to the regular periodic MMOs, chaotic oscillations, simple relaxations, or small amplitude oscillations. Various bifurcation diagrams show the fractal nature of the local maximum sequences. Graphical representation of those sequences results in special two-dimensional windows trees (Figs. 12–13). Also, the hierarchical oscillatory sequences have their fractal dimensions very close to those of the Ford circles and possibly other similar structures (e.g. the Cantor set complementary to the devil's staircase associated with the circle map [4]). We estimate the fractal dimensions of our circuits to be $\sim$2.52 (capacity dimension, formula (6)), 2.38–2.49 (modified Kaplan–Yorke dimension, formula (10)) and 2.26–2.36 (Kaplan–Yorke dimension, formula (9)).

The circuits considered in this paper, while simple in their structures, show a very rich spectrum of dynamical properties. This makes the circuits quite intriguing, not only from the point of view of the bifurcation oscillations following the Farey sequence of coprime integers, but also from the point of view of fractal properties, interaction of oscillators and singularly perturbed circuits. The *jerk* Newtonian variable x_1 relates the circuits to Newton's law $x_1'' = F/m$ where x_1'' is the "acceleration"

[2]For a polynomial *jerk* equation $x''' = J(x'', x', x)$, the $J(x'', x', x)$ must be a polynomial function of all three variables x, v and a with $v = x'$ and $a = x''$ [5, Appendix B].

given by (13). It is expected that the circuits, considered as a coupling of oscillators (through the K element), may also show the mode entrainment phenomenon leading to the existence of the mode locking Arnold's tongues.

Acknowledgements The author would like to thank the anonymous reviewers for their constructive comments and Dr. M.N.S. Swamy, Editor-in-Chief, for his helpful assistance in the review process. This work was done while the author was on a sabbatical at Martin Luther University in Halle–Wittenberg (Germany). Financial support of the Alexander von Humboldt Foundation is greatly appreciated.

References

1. R.E. Beardmore, R. Laister, The flow of a differential-algebraic equation near a singular equilibrium. SIAM J. Matrix Anal. **24**, 106–120 (2002)
2. M. Brøns, M. Krupa, M. Wechselberger, Mixed mode oscillations due to the generalized canard phenomenon. Fields Inst. Commun. **49**, 39–63 (2006)
3. K.E. Chlouverakis, J.C. Sprott, A comparison of correlation and Lyapunov dimensions. Physica D **200**, 156–164 (2005)
4. S. De Brouwer, D.H. Edwards, T.M. Griffith, Simplifications of the quasiperiodic route to chaos in agonist-induced vasomotion by iterative circle maps. Am. J. Physiol. **274**, H1315–H1326 (1998)
5. R. Eichhorn, S.J. Linz, P. Hänggi, Transformations of nonlinear dynamical systems to jerky motion and its application to minimal chaotic flows. Phys. Rev. E **58**, 7151–7164 (1998)
6. Focus issue: Mixed mode oscillations: experiment, computation, and analysis. Chaos **18**(1) (2008)
7. L.R. Ford, Fractions. Am. Math. Mon. **45**, 586–601 (1938)
8. J.G. Freire, J.A.C. Gallas, Stern–Brocot trees in cascades of mixed-mode oscillations and canards in the extended Bonhoeffer–van der Pol and FitzHugh–Nagumo models of excitable systems. Phys. Lett. A **375**, 1097–1103 (2011)
9. M. Krupa, N. Popovic, N. Kopell, Mixed-mode oscillations in three time-scale systems: a prototypical example. SIAM J. Appl. Dyn. Syst. **7**, 361–420 (2008)
10. M. Krupa, P. Szmolyan, Relaxation oscillation and canard explosion. J. Differ. Equ. **174**, 312–368 (2001)
11. R.B. Leipnik, T.A. Newton, Double strange attractors in rigid body motion with linear feedback control. Phys. Lett. A **86**, 63–67 (1981)
12. S.J. Linz, Newtonian jerky dynamics: some general properties. Am. J. Phys. **66**, 1109–1114 (1998)
13. W. Marszalek, Fold points and singularities in Hall MHD differential-algebraic equations. IEEE Trans. Plasma Sci. **37**, 254–260 (2009)
14. W. Marszalek, T. Amdeberhan, R. Riaza, Singularity crossing phenomena in DAEs: a two-phase fluid flow application case study. Comput. Math. Appl. **49**, 303–319 (2005)
15. W. Marszalek, Z. Trzaska, Singularity-induced bifurcations in electrical power systems. IEEE Trans. Power Syst. **20**, 312–320 (2005)
16. W. Marszalek, Z. Trzaska, Mixed-mode oscillations in a modified Chua's circuit. Circuits, Systems. Signal Process. **29**, 1075–1087 (2010)
17. J. Maselko, L. Swinney, Complex periodic oscillations and Farey arithmetic in the Belousov–Zhabotinskii reaction. J. Chem. Phys. **85**, 6430–6441 (1986)
18. B. Munmuangsaen, B. Srisuchinwong, J.C. Sprott, Generalization of the simplest autonomous chaotic system. Phys. Lett. A **375**, 1445–1450 (2011)
19. V. Petrov, S.K. Scott, K. Showalter, Mixed-mode oscillations in chemical systems. J. Chem. Phys. **97**, 6191–6198 (1992)
20. L. Pivka, C.W. Wu, A. Huang, Chua's oscillator: a compendium of chaotic phenomena. J. Franklin Inst. **331B**, 705–741 (1994)
21. R. Riaza, S.L. Campbell, W. Marszalek, On singular equilibria of index-1 DAEs. Circuits Syst. Signal Process. **19**, 131–157 (2000)
22. J.C. Sprott, A new chaotic jerk circuits. IEEE Trans. Circuits Syst. II, Express Briefs. **58**, 240–243 (2011)

23. M. Wechselberger, Existence and bifurcations of canards in R^3 in the case of a folded node. SIAM J. Appl. Dyn. Syst. **4**, 101–139 (2005)
24. N.J. Wildberger, Evolution versus intelligent design: a mathematician's view. http://web.maths.unsw.edu.au/norman/papers/IntelligentDesignhtml/IntelligentDesign1.htm (2008). Accessed 19 Dec. 2011
25. X.-X. Xu, S.-J. Ma, P.-T. Huang, New concepts in electromagnetic jerky dynamics and their applications in transient processes of electric circuit. Prog. Electromagn. Res. M. **8**, 181–194 (2009)